Electron-Impact Ionization of Neon at Low Projectile Energy: An Internormalized Experiment and Theory for a Complex Target

Thomas Pflüger,[2,1,*] Oleg Zatsarinny,[3] Klaus Bartschat,[3] Arne Senftleben,[2] Xueguang Ren,[2,1] Joachim Ullrich,[1,2] and Alexander Dorn[2]

[1]*Physikalisch-Technische Bundesanstalt, Bundesallee 100, 38116 Braunschweig, Germany*
[2]*Max-Planck-Institut für Kernphysik, Saupfercheckweg 1, 69117 Heidelberg, Germany*
[3]*Department of Physics and Astronomy, Drake University, Des Moines, Iowa 50311, USA*

(Received 24 January 2013; published 9 April 2013)

As a fundamental test for state-of-the-art theoretical approaches, we have studied the single ionization ($2p$) of neon at a projectile energy of 100 eV. The experimental data were acquired using an advanced reaction microscope that benefits from high efficiency and a large solid-angle acceptance of almost 4π. We put special emphasis on the ability to measure internormalized triple-differential cross sections over a large part of the phase space. The data are compared to predictions from a second-order hybrid distorted-wave plus R-matrix model and a fully nonperturbative B-spline R-matrix (BSR) with pseudostates approach. For a target of this complexity and the low-energy regime, unprecedented agreement between experiment and the BSR model is found. This represents a significant step forward in the investigation of complex targets.

DOI: 10.1103/PhysRevLett.110.153202 PACS numbers: 34.80.Gs

Charged-particle interactions with atoms and molecules represent a fundamental process in physics that has been studied for decades. In particular, reactions involving electrons are of widespread importance for many applications in fundamental, technological, and even medical research. The most detailed information about the dynamics of a single-ionization process is found in $(e, 2e)$ experiments, pioneered by the work of Ehrhardt *et al.* [1]. In these kinematically complete experiments, the entire momentum information for both final-state electrons is recorded. From the start of this type of studies, simple targets (e.g., atomic hydrogen and helium) have been investigated over a wide range of projectile energies. Simultaneously, theoretical models were developed to describe these processes. In the beginning, these were perturbative approaches (such as the first-order plane-wave Born approximation), which had great difficulties in reproducing the experimental data even for these simple systems at low impact energies.

The study of more complex targets (e.g., neon, argon, etc.) imposed additional problems in the description of the target structure. Major theoretical advancements in handling such systems include the distorted-wave Born approximation by Madison *et al.* [2] as well as the first-order (DWB1-RM) and later second-order (DWB2-RM) hybriddistorted-wave + R-matrix approach by Bartschat and collaborators [3–5]. In the latter, the projectile-target interaction is accounted for perturbatively, while the initial bound state and the ejected-electron–residual-ion scattering process is described nonperturbatively via a close-coupling (R-matrix) expansion. However, problems for the low-energy regime prevailed due to a less than ideal (if any) description of the postcollision interaction (PCI) between the two outgoing electrons. Attempts to fix this problem include the use of asymptotically correct three-body wave functions in the 3DW approach [6] or the *ad hoc* introduction of some version of the Gamov factor [7]. While these methods have occasionally been successful, serious problems include the fact that the 3DW wave function may not be sufficiently accurate at small distances between the projectile and the target (where the ionization occurs), while the Gamov factor is known to be very problematic regarding the overall normalization. Neither of these methods has been shown to yield a systematic and predictable improvement in the general case.

Recent rapid developments in computational resources marked the onset of nonperturbative approaches that attempt the solution of the Schrödinger equation limited only by numerical aspects. Implementations such as the convergent-close-coupling [8] and the time-dependent-close-coupling [9] methodology have been highly successful in the low-energy regime for the ionization of H-like and He-like targets, albeit in the latter case with the restriction of the second bound electron remaining in the $1s$ orbital. While a few attempts have been made to apply these methods in the single-active-electron approach to other targets (e.g., Refs. [10,11]), it is not clear how accurate the results might be in light of the necessary approximations made in the structure description.

The major void to be filled, therefore, concerns the intermediate- to low-energy electron interaction with complex targets. Recent efforts include experiments at 150 eV projectile energy for the $2p$ ionization of neon in the coplanar geometry [12]. These results were put on an absolute scale by using helium as a reference target, whose cross section scale was derived from convergent-close-coupling calculations [13]. Due to the nature of the

 © 2013 American Physical Society

experiment, only a limited number of scattering angles were presented for a single ejection energy. Comparison with distorted-wave Born approximation and DWB2-RM resulted in an overall reasonable agreement, although significant differences in the cross-section magnitude remained.

The recently developed B-spline R-matrix (BSR) with pseudostates method aims to fill the gap via a fully nonperturbative treatment of the $(e, 2e)$ process for complex target atoms. It achieved a breakthrough in the vastly improved description of the highly correlated process of ionization with simultaneous excitation in helium [14], and the approach was further validated in an extensive study for $(e, 2e)$ on helium leaving the residual ion in the He^+ $(1s)$ ground state [15]. When applied to electron-impact ionization of argon [16,17], an unprecedented reproduction of the experimentally observed cross-section patterns as a function of emission angle for the slow electron at fixed electron energies was also observed. On the other hand, open questions remained concerning the dependence of the cross-section magnitude as a function of the projectile scattering angle. A recent reconsideration of the data analysis procedure on the experimental side, however, revealed that this issue, to a large extent, can be assigned to a missing solid-angle correction factor in processing the raw data [18].

In the present work a comprehensive study for electron-impact single ionization of atomic neon's $2p$-orbital with a projectile energy of $E_0 = 100$ eV is performed. We not only compare the angular dependence of the individual triple-differential cross section (3DCS) but also make use of the experiment's capability to internormalize the measurements for different kinematical situations. Furthermore, the possibility of covering a large part of the final-state phase space simultaneously in a single experiment provides an ideal test ground for theory. The measurements reported here cover a range of ejected-electron energies ($E_{e2} = 2$ eV, 5 eV, 8 eV, 16.5 eV) and projectile scattering angles ($\theta_{e1} = -5°, -10°, -15°, -20°$).

The experimental side of this work was carried out by employing an advanced reaction microscope. This technique was described in detail elsewhere (see, for example, Refs. [19,20]). Briefly, a focused pulsed electron beam from a thermocathode is crossed with a target beam created by supersonic expansion of gaseous neon at room temperature. The target creation involves a three-stage pumping system, producing a well-collimated beam of cold (~ 2 K) atoms. By means of homogeneous electric and magnetic fields the residual ion and the two final-state electrons e_1 and e_2 are projected onto time- and position-sensitive detectors. A hole in the center of the electron detector required to dump the unscattered primary beam defines a lower limit for detectable polar angles with respect to the spectrometer axis, while for the azimuthal range full acceptance is achieved. In detail, the polar acceptance is $\theta_{e2}(E_{e2}=2\text{eV})=[43°,137°]$, $\theta_{e2}(E_{e2}=5\text{eV})=[27°,153°]$, $\theta_{e2}(E_{e2}=8\text{ eV})=[22°,158°]$, and $\theta_{e2}(E_{e2}=16.5\text{eV})=[18°,164°]$. From the individually measured time-of-flight and position of each particle the three-dimensional momentum vector is calculated. Thus, full three-dimensional 3DCS are accessible. Since the complete experimentally accessible phase space is measured simultaneously, all relative 3DCS are cross normalized and only a single global factor is required in comparison of theory and experiment. This factor is used to put the 3DCS on an absolute scale.

The calculations for this work were carried out following the methodology described in several recent papers [14,15,17]. For the neon target, we used the 679-state nonrelativistic BSR model developed for another calculation [21] to describe elastic scattering and electron-impact excitation at intermediate energies. Of the 679 states in our close-coupling expansion, 55 states represent the bound spectrum and the remaining 624 the target continuum. We included all singlet and triplet target states with total electronic angular momentum $L = 0$–4. The continuum pseudostates in the present calculations cover the energy region up to 85 eV.

The R-matrix radius was set to $30a_0$, where $a_0 = 0.529 \times 10^{-10}$ m is the Bohr radius. We employed 70 B-splines to span this radial range using a semi-exponential knot grid. The scattering model contained up to 2,280 scattering channels, leading to generalized eigenvalue problems with matrix dimensions up to 150,000 in the B-spline basis that is used for the expansion of the outer target orbitals (including the pseudoorbitals) as well as the projectile wave function inside the R-matrix box. We calculated partial waves for total orbital angular momenta $L \leq 25$ numerically and then used a top-up procedure to estimate the contributions from even higher L values.

The ionization amplitudes were determined by the projection method described in detail in Ref. [15]. This is a two-step process, in which the scattering amplitudes for excitation of the pseudostates are mapped to true continuum states of the ejected-electron–residual-ion system through overlap factors between the pseudostates and these continuum states, which are generated by performing a separate close-coupling calculation for electron scattering from Ne^+. We obtain numerically stable results if the latter close-coupling expansion is the same as the one used to obtain the pseudostates in the frozen-core bound-state approach. The only difference between the latter and the collision calculation are the boundary conditions at large distances away from the target, where the bound states have to vanish. Specifically, we used a two-state expansion for this part of the problem, including the $(2s^2 2p^5)^2P$ and $(2s2p^6)^2S$ states of Ne^+. Note that the BSR approach with individually optimized, and hence nonorthogonal, orbital sets allows for an accurate representation of these ionic states.

In Fig. 1 a three-dimensional 3DCS pattern is exhibited for a projectile scattering angle of $-10°$ and 8 eV energy of the ejected electron. The left panel represents the measured data while the BSR prediction is shown on the right. In this particular representation, the relative 3DCS is given by the radial distance from the origin to the surface of the plot. The projectile with momentum $\boldsymbol{p}_0$ enters the interaction region from below and after scattering has the momentum $\boldsymbol{p}_{e1}$. The momentum transfer to the target system is indicated by the arrow labeled $\boldsymbol{q}$. Two general features are observable. Electrons emitted roughly in the direction of the momentum transfer form the binary peak, while those emitted in the opposite direction form the recoil peak.

Here, the binary peak exhibits a pronounced dip in the direction of $\boldsymbol{q}$. This is the result of the characteristic momentum profile of a p-orbital that has a node for vanishing momentum. Therefore, the binary peak in Fig. 1 exhibits a maximum cross section for electron emission on a cone around the $\boldsymbol{q}$ direction. Due to the low energy of the projectile, PCI is strong (as expected) and, consequently, the binary peak is suppressed near the forward direction. The qualitative comparison of experiment and theory shows very good overall agreement, with the suppression of the binary peak towards the forward direction being slightly more pronounced in the experimental data.

Furthermore, three planes are indicated in Fig. 1, which will be used to compare experiment and theory quantitatively in Fig. 2. Those are the xz plane or scattering plane (continuous), the yz plane or perpendicular plane (dash-dotted), and the xy plane or full-perpendicular plane (dashed). The kinematical conditions studied for Fig. 2 correspond to scattering angles of the projectile from $\theta_{e1} = -5°$ to $-20°$ (top to bottom) for ejection energies $E_{e2} = 2$ eV [(a)–(d)], $E_{e2} = 5$ eV [(e)–(h)], $E_{e2} = 8$ eV [(i)–(l)], and $E_{e2} = 16.5$ eV [(m)–(p)], respectively. The global scaling factor used to normalize the experimental data to the BSR theory was found by achieving the best fit to the binary peak for the 8 eV, $-10°$ case shown in Figure 2(j). It was subsequently applied to all other kinematics and planes.

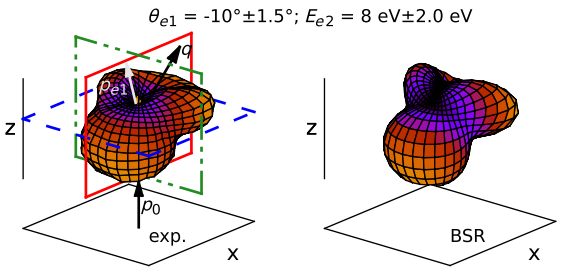

FIG. 1 (color online). Three-dimensional triple-differential cross section for $2p$ ionization of neon. The experimental pattern on the left is compared with the BSR predictions on the right. The scattering angle is $\theta_{e1} = -10° \pm 1.5°$, and the ejection energy is $E_{e2} = 8$ eV $\pm$ 2.0 eV.

We begin the discussion with the left column of Fig. 2, which presents the 3DCS within the scattering plane as a function of the polar angle of the emitted electron θ_{e2} for different scattering angles of the projectile θ_{e1} and ejection energies E_{e2}. The experimental data are compared to predictions from the DWB2-RM and BSR models. The scattering plane cuts through the binary and the recoil peaks and contains the momentum transfer vector indicated by an arrow. As seen in the figure, a high degree of agreement between BSR and the experimental data is achieved for many cases—not only regarding the angular dependence of the cross sections but also the relative magnitude over the entire range of angle and energy conditions analyzed. We generally observe the well-known behavior that for increasing projectile scattering angle θ_{e1} and, therefore, increasing momentum transfer, the binary peak gets stronger compared to the recoil peak. This is particularly clear for the larger emission energies of $E_{e2} = 8$ eV [panels (i)–(l)] and $E_{e2} = 16.5$ eV [panels (m)–(p)]. We also find that the influence of PCI on the binary peak pattern, which was mentioned above, varies with the projectile scattering angle θ_{e1}. Due to the characteristic dip along the $\boldsymbol{q}$ direction, the binary peak is split in this representation, with one peak at smaller and one at larger angles with respect to $\boldsymbol{q}$. When the projectile scattering angle θ_{e1} approaches zero degrees (for a fixed ejection energy E_{e2}), the momentum transfer is shifted to smaller angles. Consequently, electrons emitted in the direction of the binary peak are in close vicinity to the scattered projectile and hence PCI is enhanced. This can be exemplified for the cases with $E_{e2} = 8$ eV [panels (i)–(l)]: Going from the bottom panel to the top, θ_{e1} decreases and the binary peak—as a whole—is shifted towards smaller θ_{e2}. In addition, emission to the part of the binary peak at small angles with respect to $\boldsymbol{q}$ is becoming strongly suppressed. The BSR model is able to reproduce this behavior. The DWB2-RM, on the other hand, does not include PCI and predicts no such suppression of the cross section. The best agreement between experiment and the BSR results is seen for $E_{e2} = 5$ eV and 8 eV. For $E_{e2} = 16.5$ eV PCI should be strongest since this case has the most symmetric energy sharing of the data sets presented. Here, the forward binary lobe is not visible experimentally even for the largest $\theta_{e1} = -20°$, whereas BSR shows a fairly small peak. Generally, BSR seems to slightly overestimate the binary forward lobe compared to experiment. The most significant disagreement between experiment and the BSR results is encountered for $E_{e2} = 2$ eV, where deviations in the magnitude of the large angle binary lobe are visible for the two smallest θ_{e1} angles.

For the perpendicular plane exhibited in the center part of Fig. 2, a three-lobe pattern is evident. This plane cuts through the double-lobe binary peak, thereby resulting in two symmetric maxima in the ranges $\theta_{e2} = 60°$–$90°$ and $\theta_{e2} = 270°$–$300°$, respectively. In addition

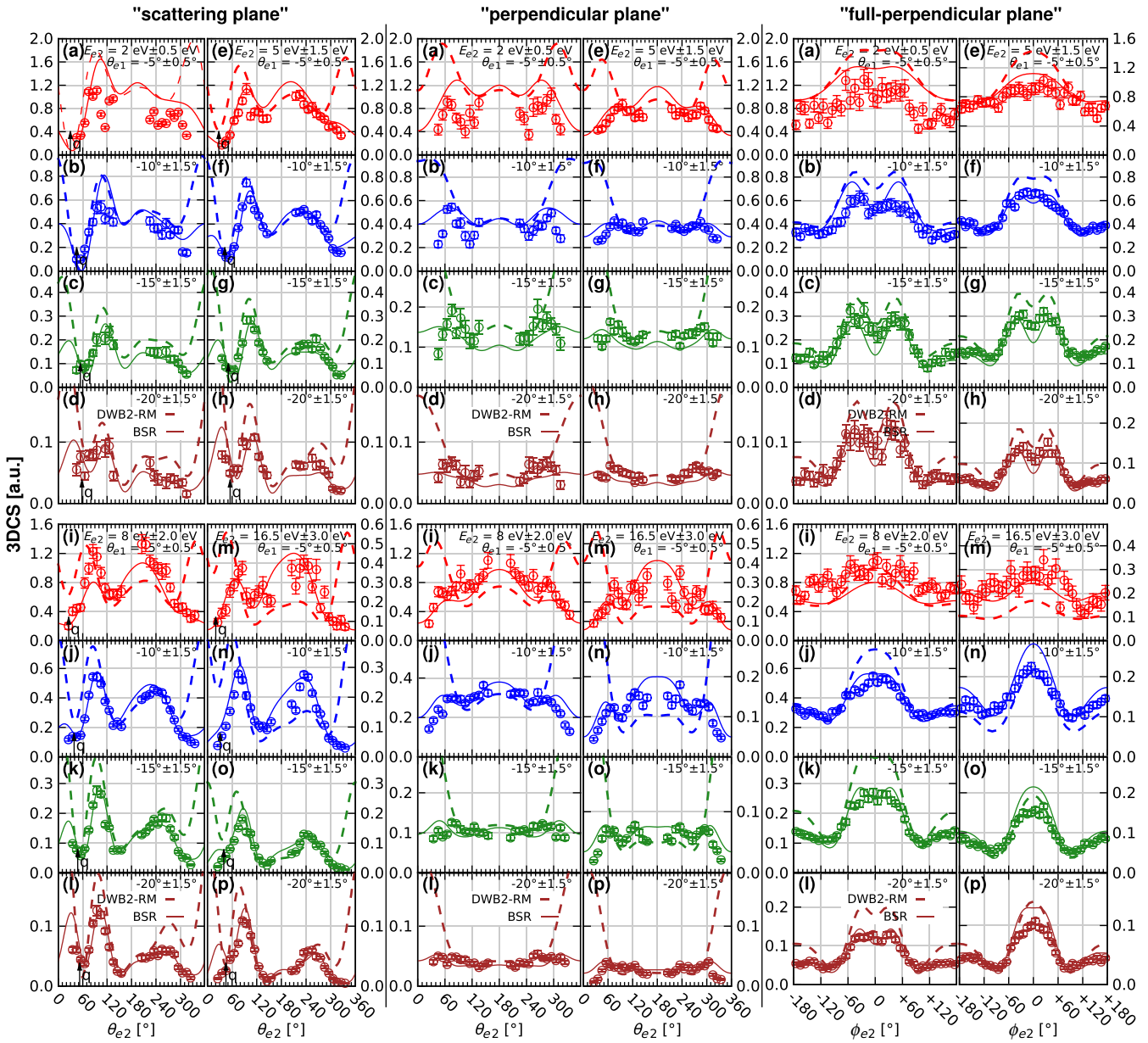

FIG. 2 (color online). 3DCS Ne($2p$) for ejection energies (columns) $E_{e2} = 2$ eV $\pm$ 0.5 eV [(a)–(d)], $E_{e2} = 5$ eV $\pm$ 1.5 eV [(e)–(h)], $E_{e2} = 8$ eV $\pm$ 2.0 eV [(i)–(l)] and $E_{e2} = 16.5$ eV $\pm$ 2.0 eV [(m)–(p)] for scattering angles of $\theta_{e1} = -5° \pm 0.5°$, $-10° \pm 1.5°$, $-15° \pm 1.5°$ and $-20° \pm 1.5°$ (top to bottom). The left panels are for the coplanar geometry, the center panels for the perpendicular plane, and the right panels for the full-perpendicular plane. Continuous line: BSR model, dashed line: DWB2-RM. Error bars denote the statistical error of the data.

the recoil lobe gives rise to the central maximum at $\theta_{e2} = 180°$. In this plane PCI acts strongest for small angles near $\theta_{e2} = 0°$, 360°. Once again, generally good agreement is found between the BSR results and the experimental data. This is of particular importance, as the correct description of the cross section in the perpendicular plane has been a difficult problem in the past. Here deviations between theory—which did well in the scattering plane—and experiment were found to be large (see, for example, Refs. [22,23]). For the present study, we again find the largest deviations for the smallest ejection energy of $E_{e2} = 2$ eV, where the data exhibit pronounced dips in the 120°/240° direction. For $E_{e2} = 5$ eV the agreement is already quite good, although the magnitude of the experimental data and the BSR predictions deviates for the two largest scattering angles (i.e., $\theta_{e1} = -15°$ and $-20°$). As the energy E_{e2} increases, these deviations diminish. At the highest energy of $E_{e2} = 16.5$ eV, excellent agreement is obtained for essentially all scattering angles.

We finish by considering the full-perpendicular plane, which is perpendicular to the projectile momentum vector $\boldsymbol{p}_0$ (right column of Fig. 2). In this geometry the ejected electron's polar angle is fixed to $\theta_{e2} = 90°$. Now the azimuthal angle ϕ_{e2} is plotted with the projectile's radial component $p_{r,e1}$ at 0°. The central double-hump maximum originates from the binary peak, while the maximum, which in many cases is seen at $\theta_{e2} = -180°$, 180°, is caused by the recoil peak. In this plane the influence of PCI is rather small for all angles ϕ_{e2}. Consequently, the differences between the BSR and the DWB2-RM results are only moderate albeit certainly not negligible. Overall, the agreement between experiment and the BSR predictions is significantly better than with DWB2-RM.

We have presented kinematically complete electron-impact ionization experiments of the $2p$-orbital of neon at a projectile energy of 100 eV. For 16 different kinematical cases, internormalized cross sections were obtained in order to critically test a semiperturbative hybrid second-order distorted-wave plus R-matrix model as well as a state-of-the-art fully nonperturbative BSR approach. The DWB2-RM model provides reasonable cross sections for ionization geometries where PCI does not play a significant role. As expected, however, it fails in regions with small mutual emission angle and, thus, strong PCI between the two final-state continuum electrons. The experimental data and the BSR results, on the other hand, reveal an unprecedented degree of agreement not only in shape but also in the relative magnitude of the triple-differential cross section over a significant range of scattering angles and ejection energies. This study represents an important step—experimentally as well as theoretically—towards the understanding of the ionization of complex atomic targets at low impact energies.

T. P. would like to thank M. Schulz for his valuable input. This work was supported, in part, by the Deutsche Forschungsgemeinschaft (DFG) under Project No. RE 2966/1-1 (X. R.) and the United States National Science Foundation under Grants No. PHY-1068140 and No. PHY-1212450 (O. Z. and K. B.). The BSR computations were carried out on Lonestar at the Texas Austin Computer Center. They were made possible through the XSEDE allocation PHY-090031.

*thomas.pflueger@mpi-hd.mpg.de

[1] H. Ehrhardt, M. Schulz, T. Tekaat, and K. Willmann, Phys. Rev. Lett. **22**, 89 (1969).
[2] D. H. Madison, R. V. Calhoun, and W. N. Shelton, Phys. Rev. A **16**, 552 (1977).
[3] K. Bartschat and P. G. Burke, J. Phys. B **20**, 3191 (1987).
[4] R. H. G. Reid, K. Bartschat, and A. Raeker, J. Phys. B **31**, 563 (1998).
[5] Y. Fang and K. Bartschat, J. Phys. B **34**, L19 (2001).
[6] A. Prideaux and D. H. Madison, Phys. Rev. A **67**, 052710 (2003).
[7] S. J. Ward and J. H. Macek, Phys. Rev. A **49**, 1049 (1994).
[8] I. Bray, Phys. Rev. Lett. **89**, 273201 (2002).
[9] J. Colgan, M. S. Pindzola, F. J. Robicheaux, D. C. Griffin, and M. Baertschy, Phys. Rev. A **65**, 042721 (2002).
[10] C. P. Ballance, J. A. Ludlow, M. S. Pindzola, and S. D. Loch, J. Phys. B **42**, 175202 (2009).
[11] K. Bartschat, D. V. Fursa, and I. Bray, J. Phys. B **43**, 125202 (2010).
[12] L. R. Hargreaves, M. A. Stevenson, and B. Lohmann, J. Phys. B **43**, 205202 (2010).
[13] L. R. Hargreaves, M. A. Stevenson, and B. Lohmann, Meas. Sci. Technol. **21**, 055112 (2010).
[14] O. Zatsarinny and K. Bartschat, Phys. Rev. Lett. **107**, 023203 (2011).
[15] O. Zatsarinny and K. Bartschat, Phys. Rev. A **85**, 062709 (2012).
[16] X. Ren, T. Pflüger, J. Ullrich, O. Zatsarinny, K. Bartschat, D. H. Madison, and A. Dorn, Phys. Rev. A **85**, 032702 (2012).
[17] O. Zatsarinny and K. Bartschat, Phys. Rev. A **85**, 032708 (2012).
[18] X. Ren, T. Pflüger, J. Ullrich, O. Zatsarinny, K. Bartschat, D. H. Madison, and A. Dorn (to be published).
[19] J. Ullrich, R. Moshammer, A. Dorn, R. Dörner, L. Schmidt, and H. Schmidt-Böcking, Rep. Prog. Phys. **66**, 1463 (2003).
[20] X. Ren, A. Senftleben, T. Pflüger, A. Dorn, K. Bartschat, and J. Ullrich, J. Phys. B **43**, 035202 (2010).
[21] O. Zatsarinny and K. Bartschat, Phys. Rev. A **86**, 022717 (2012).
[22] M. Schulz, R. Moshammer, D. Fischer, H. Kollmus, D. H. Madison, S. Jones, and J. Ullrich, Nature (London) **422**, 48 (2003).
[23] X. Ren, I. Bray, D. V. Fursa, J. Colgan, M. S. Pindzola, T. Pflüger, A. Senftleben, S. Xu, A. Dorn, and J. Ullrich, Phys. Rev. A **83**, 052711 (2011).